J. Biophotonics **4**, No. 5, 297–304 (2011) / **DOI** 10.1002/jbio.201000059

Journal of BIOPHOTONICS

FULL ARTICLE

Two-photon microscopy of healthy, infarcted and stem-cell treated regenerating heart

Marika A. Wallenburg[1], *Jun Wu*[2], *Ren-Ke Li*[2], *and I. Alex Vitkin*[*,3]

[1] Ontario Cancer Institute, Division of Biophysics and Bioimaging, University Health Network and University of Toronto, Department of Medical Biophysics, 610 University Avenue, Toronto, ON, M5G 2M9, CANADA
[2] Toronto General Research Institute, Division of Cardiovascular Surgery, University Health Network and University of Toronto, Toronto, Ontario, Canada, 610 University Avenue, Toronto, ON, M5G 2M9, CANADA
[3] Ontario Cancer Institute, Division of Biophysics and Bioimaging, University Health Network and University of Toronto, Departments of Medical Biophysics and Radiation Oncology, 610 University Avenue, Toronto, ON, M5G 2M9, CANADA

Received 21 April 2010, revised 11 July 2010, accepted 19 August 2010
Published online 7 September 2010

Key words: myocardial infarction, two-photon fluorescence, second-harmonic generation, collagen

Two-photon excitation autofluorescence (produced in myocytes) and second-harmonic generation (produced mainly by collagen) allow label-free visualization of these two important components of myocardium. Because of their different emission wavelengths, these two signals can be separated spectrally. Here, we examine two-photon microscopy images of healthy, infarcted and stem-cell treated rat hearts. We find that in infarcted heart, regions distant from the site of infarct are similar to healthy tissue in composition (mostly myocytes, very little collagen) and organization (densely packed myocytes), but infarct regions are characterized by sparse myocytes and high collagen content indicative of scar tissue formation. Stem cell treated hearts, in contrast, show regions of intertwined myocytes and collagen throughout the infarct, suggesting reduced tissue damage. Finally, these results offer interesting insights into our ongoing polarized light studies of cardiac tissue anisotropy, and reveal that both tissue composition and tissue micro-organization are reflected in polarization-measured linear retardance values.

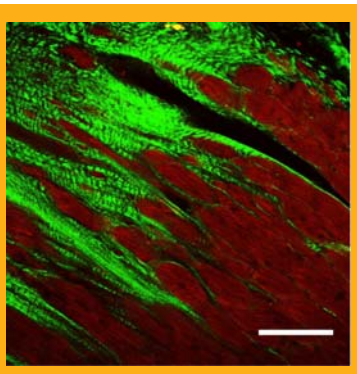

Second harmonic generation (green) and two-photon autofluorescence (red) allow simultaneous visualization of the collagen and myocyte components of stem-cell treated infarcted rat myocardium. Scale bar = 100 μm

1. Introduction

Two-photon microscopy (TPM) has recently become a widely-used tissue assessment tool, as it offers many advantages over confocal microscopy and histology. While maintaining the high resolution of confocal microscopy, TPM has the added benefits of intrinsic depth-sectioning, no out-of-focus bleaching, and relatively high depth penetration. Furthermore, many endogenous molecules can serve as sources of signal for TPM, eliminating the need for labels and stains for certain applications. For instance, two-photon ex-

* Corresponding author: e-mail: vitkin@uhnres.utoronto.ca, Phone: (416) 946-2990, Fax: (416) 946-6566

citation autofluorescence (TPEF) allows imaging of endogenous fluorescent structures such as extracellular matrix (elastin [1, 2]) and myocytes [2, 3]. Second harmonic generation (SHG), another non-linear optical process, is generated by non-centrosymmetric molecules, including collagen [1, 2, 4] and myosin [3, 5, 6]. Specifically, the potential of two-photon microscopy is well established in cardiology: it has been performed on whole (healthy and diseased) mouse hearts [7, 8], on diseased human and porcine heart valve tissues [9], on human atrial myocardium [10], and on perfused ischemic rat hearts [11]. However, it has not yet been used to examine infarcted and regenerating myocardium. Two-photon microscopy is particulaly well suited for this application because of the distinct mechanisms (SHG and TPEF) which allow, through spectral decomposition, simultaneous and intrinsically co-registered visualization of the two main components of infarcted myocardium, namely cardimyocytes and collagen.

Here, we report on the use of simultaneous two-photon autofluorescence and second-harmonic generation to image both the collagen and the myocyte content of healthy, infarcted and regenerating (stem-cell treated) rat hearts, yielding information on both the extracellular matrix and the muscle cell components of heart. These qualitative results reveal interesting microstructural and compositional features with the potential to verify biological hypotheses regarding the mechanisms of stem cell regeneration. Furthermore, these provide insight for interpretation of our ongoing polarized-light-based tissue anisotropy studies and reveal the effect of tissue composition (myocytes versus collagen), organization (fibrillar versus wavy collagen) and orientation (anisotropy axis alignment).

2. Methods

2.1 Samples: Rat heart infarct/regeneration model

All animal studies were performed at the Toronto General Hospital and carried out under institutional approval from the University Health Network (Toronto, Canada). The cardiac samples were from a Lewis rat model of myocardial infarction. The first group of rats ($n = 5$) underwent permanent left anterior descending (LAD) coronary artery ligation, and the animals were sacrificed nine weeks post ligation (see Table 1). The second group ($n = 4$) underwent the same coronary ligation, but were treated one week later with mesenchymal stem cells transfected with human elastin gene, administered by intramyocardial injection at the site of infarct [12]. These animals were also sacrificed nine weeks after LAD ligation induced infarction. A third group of healthy rats ($n = 2$) was used as a control. The hearts were excised, fixed in 10% formalin, and sectioned axially to either 0.5, 1, or 2 mm thickness (see Figure 1a). The final thickness of the samples has no effect on our results, as imaging was performed only in the first ≈ 50 mm layer of tissue where signal was strongest. After two-photon imaging, histology was done on one sample of each group with Masson's Trichromne staining: collagen and connective tissue are stained blue, cytoplasm in pink, and nuclei in dark red.

2.2 Multiphoton microscopy

Multiphoton microscopy was performed using a Zeiss LSM 510 META NLO microscope and a tunable Chameleon Ti : Sapphire laser (720–930 nm) set to an excitation wavelength of 840 nm. A 20×0.75 NA dry objective was used. Second-harmonic and two-photon fluorescence signals were recorded in the backscattered direction and spectrally decomposed on a META spectral detector. Note that because of the presence of a pinhole on the collection end, the light reaching the META detector is highly collimated, and tissue scattering should therefore not affect wavelength registration as scattered photons will generally not be detected. SHG signal was recorded between 400–430 nm (displayed in green pseudocolor). The images produced by TPEF collected over different wavelength ranges (430–460 nm, 460–490 nm, 490–520 nm) change very little (see discussion in next section); hence, the 430–460 nm range was used here (displayed in red pseudocolor). Each 1024×1024 pixel (460×460 μm) region took 31 seconds to scan, with each line averaged 8 times to increase signal-to-noise ratio. Multiple images were tiled to create the larger fields of view in Figures 3–5.

Table 1 Procedure and treatment undergone by each animal groups.

Group	Procedure	Treatment	End point
Myocardial infarction ($n = 5$)	LAD ligation ($t = 0$)	None	$t = 9$ weeks
Stem cell treatment ($n = 4$)	LAD ligation ($t = 0$)	Stem cell injection ($t = 1$ weeks)	$t = 9$ weeks
Healthy (control) ($n = 2$)	None	None	–

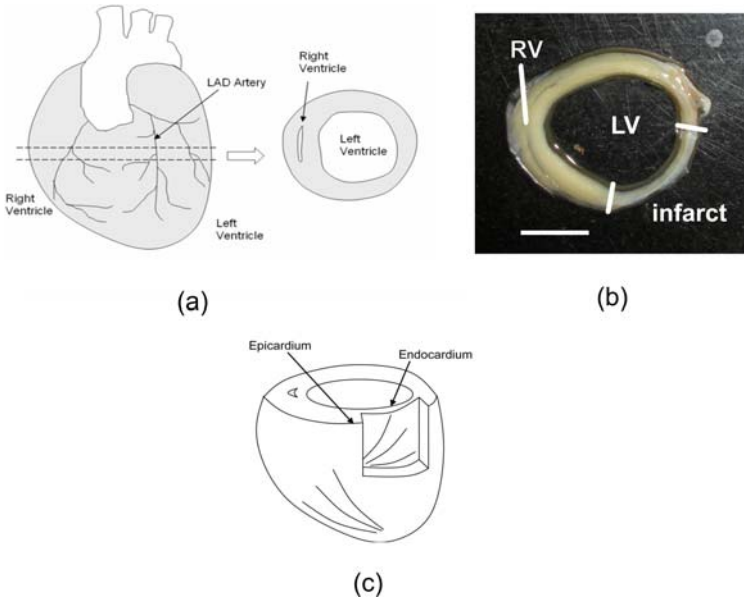

Figure 1 (online color at: www.biophotonics-journal.org) (**a**) Location of axial slices through the rat hearts, (**b**) location of infarct on one of the infarcted samples. Scale bar = 5 mm. (**c**) Change in fiber alignment from epicardium to endocardium.

3. Results

Figure 2 shows the emission spectra from two different regions of an image. The first region exhibits a sharp peak at 420 nm, which is the expected spectral signature of SHG for an excitation wavelength of 840 nm, while the second region shows very little signal at 420 nm, but rather a broad spectrum from roughly 440 nm to over 560 nm, as would be expected to result from the superposition of many individual fluorophores' spectra. The distinct, narrow peak at 420 nm and the fact that this peak shifted when the excitation wavelength was changed (always centered at half the excitation wavelength) are strong indications that the 420 nm peak represents SHG emission. Futhermore, due to the broad spectrum of the autofluorescence, we expect that if fluorescence were a significant contribution to the 400–430 nm signal, we would find positive correlation between the pixel intensities in the 400–430 nm and longer (e.g. 430–460 nm) wavelength ranges. We find no such positive correlation, which strongly suggests that fluorescence contribution to the 400–430 nm signal is negligible. For this and all subsequent images, therefore, the SHG signal was collected at 400–430 nm (displayed in green pseudocolor) and the TPEF signal was collected at 430–460 nm (displayed in red pseudocolor).

SHG signal in heart tissue has been reported from both collagen and myosin. Type I collagen is known to produce a very strong SHG signal [4, 13], with type III collagen producing a much weaker, if any, signal [14], and non-fibrillar collagen types and other extra-cellular matrix components (elastin and fibronectin) producing no signal [13, 15]. The myosin present in sarcomeres (the repeated subunit of myofibrils) also produces SHG signal [5]. In these samples, the majority of SHG production is clearly attributable to collagen, as evident from the fibrillar and non-striated aspect of the SHG-producing features in

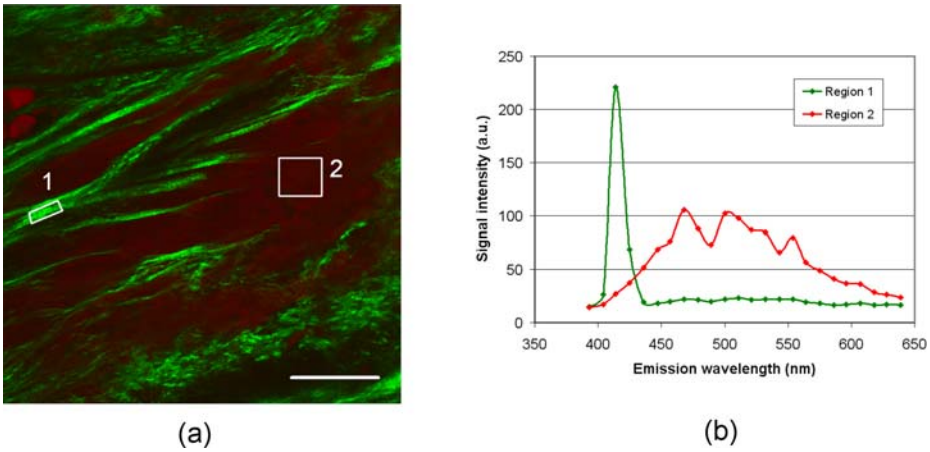

Figure 2 (online color at: www.biophotonics-journal.org) Spectral decomposition of SHG and TPEF signals for 840 nm excitation. (**a**) SHG (in green pseudocolor) is collected from 400–430 nm while TPEF (in red pseudocolor) is collected from 430–460 nm. Scale bar = 100 μm. (**b**) Emission spectra for the two regions selected in (**a**).

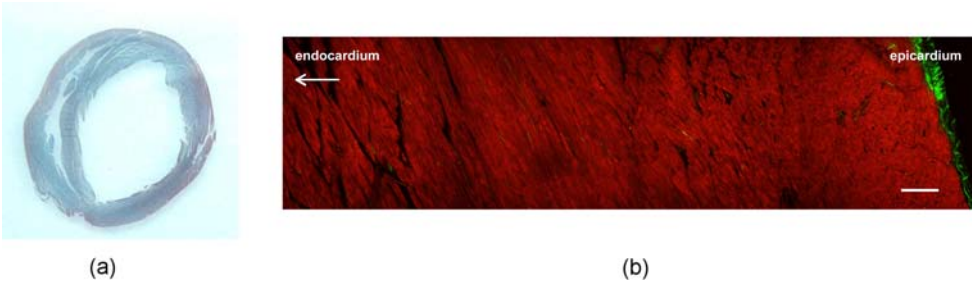

Figure 3 (online color at: www.biophotonics-journal.org) Healthy myocardium. (**a**) Histology (Masson's trichrome stain: collagen and connective tissue are stained blue, cytoplasm in pink, and nuclei in dark red). (**b**) Reprensentative two-photon microscopy image of the ventricular wall. Scale bar = 100 μm.

most images. A few SHG-producing features showing striated patterns in infarct tissue have an ambiguous source: these are discussed in more detail below. As for the two-photon autofluorescence, many endogenous fluorophores, including NADH and flavins, likely contribute to the observed signal [3, 13].

Figure 3 shows the histology and a two-photon microscopy image of healthy myocardium in the ventricular wall. There is very little collagen visible on the histology. The two-photon images also reflect this, with only a few collagen strands visible in Figure 3b. The myocytes are packed densely, and generally reflect the double-spiral structure of the heart, i.e. fibers in the mid-wall orientated circumferentially and lying in the axial (and imaging) plane, and fibers in the epicardium and endocardium oriented out of the axial plane (see Figure 1c). This is consistent with the observations of Pope et al. [16], who report a similar transmural shift in the orientation of cardiomyocytes.

Figure 4 shows histology and two-photon images from remote and infarcted regions of LAD-ligated hearts (no treatment). The histology reveals an extensive infarct and thinned ventricular walls. The infarct regions showed a high degree of sample-to-sample variation. For instance, most but not all scars were transmural. This high variation was also observed on two-photon images of the infarct regions, which revealed not only sample-to-sample variation but also high heterogeneity within different regions of a same sample. The remote regions (Figure 4b) show little collagen content and reveal myocyte orientations similar to those in Figure 3b, implying these remote regions are relatively healthy. The infarct re-

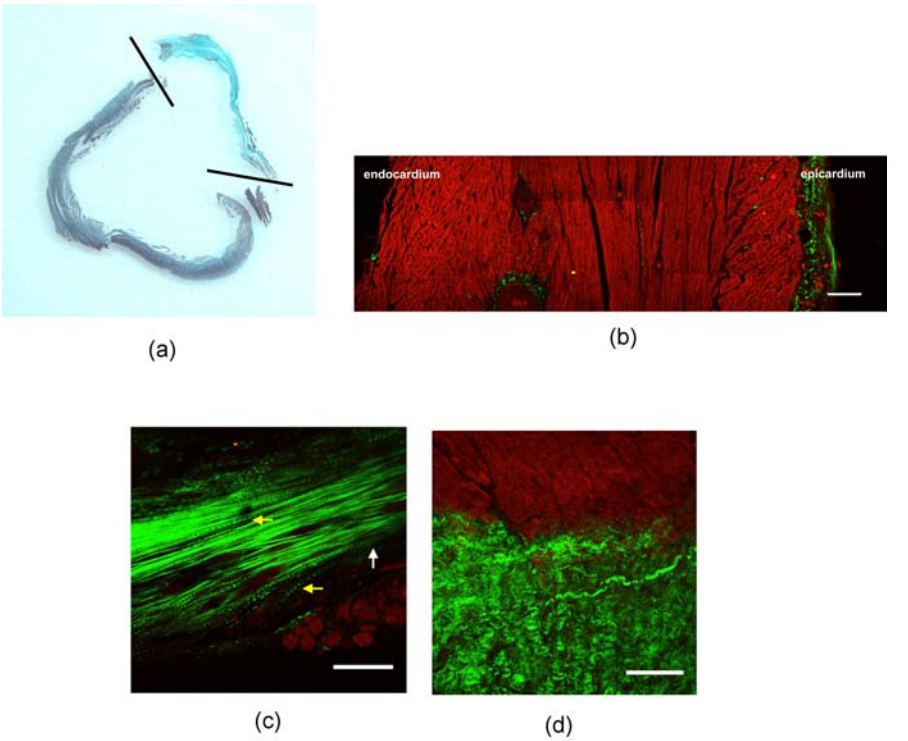

Figure 4 (online color at: www.biophotonics-journal.org) Myocardial infarction sample. (**a**) Histology (Masson's trichrome stain). The infarct is located between the bars. (**b**) Representative two-photon microscopy image of a region away from site of infarct. (**c**) Image taken from the site of infarct. Most of the SHG signal is from collagen; in a few striated regions, the SHG is due to myosin from sarcomeres (white arrow = sarcomeres); thinner, longer, or irregular striated patterns are created by collagen strands (yellow arrows = striated collagen features). (**d**) Another representative image of a site of infarct (different animal). Scale bars = 100 μm.

gions (Figure 4c and d) show lower density of myocytes than the remote regions, and considerably higher collagen content. In Figure 4c the collagen is highly linear and runs alongside a few myocytes, while in Figure 4d the collagen is more "wavy" and there is a nearly complete absence of myocytes in the collagenous region.

A few SHG features in Figure 4c present a periodicity similar to that of sarcomeres. While SHG features in Figures 3b, 4b and d can be straighforwardly identified as collagen because of their district fibrillar aspect (single, elongated strands are apparent) and/or because of the absence of striation characteristic of sarcomere, the nature of the striated patterns (see arrows in Figure 4c) is equivocal. The most regular of these patterns (white arrows) have a period of between ≈ 3–7 μm, which is slightly longer than the expected length of healthy sarcomeres (≈ 2 μm [17]), and a width of ≈ 10–20 μm, which is consistent with the width of myocytes. The longer-than-expected period of the pattern might be due to an oblique orientation of the myocyte in the plane, which would cause the observed sarcomere pattern to be longer than its true length. We note that these patterns were never visible in healthy or remote regions. The appearance of SHG signal from sarcomeres in infarcted (but not in healthy) myocytes could be due to a hyperextension of the sarcomeres in infarcted tissue: hyperextension of sarcomeric pattern has been observed in diseased myocytes [6], and the intensity of emitted SHG is known to be dependent on sarcomere length (Both et al. have shown that mice sarcomeres show a four-fold increase in SHG intensity when stretched from 2 μm to 3 μm [18]). We plan on investigating this effect further in future experiments.

Some other regular or quasi-regular SHG-producing structures visible in Figure 4c (yellow arrows), however, are too thin or too irregular to be sarcomere patterns and are more likely attributable to collagen features displaying a segmented appearance (similar to the fibers shown in [1, 10]). This appearance could arise either because of destructive interference of the SHG signal in backscatter, or because of a wavy pattern in the fiber causing the intensity of the SHG to dim periodically over the stretches where the alignment of the fiber is perpendicular to the incident light polarization (see Discussion).

Figure 5 shows histology and two-photon images of stem-cell treated rat hearts. Histology shows the extent of the scar is smaller, and the ventricular walls not as thin, as in the untreated infarct (Figure 4a), implying partial tissue remodeling. Once again, on two-photon microscopy images, the remote region (Figure 5b) shows densely packed myocytes with only a few collagen strands. Both images from the infarct region reveal a high collagen content. Figure 5c shows a region of interwoven myocytes and collagen located near the edge of the scar, while in Figure 5d the collagen forms a dense mesh around myocytes in the scar. Once again, certain periodic structures seem to be sarcomeres (white arrows). In

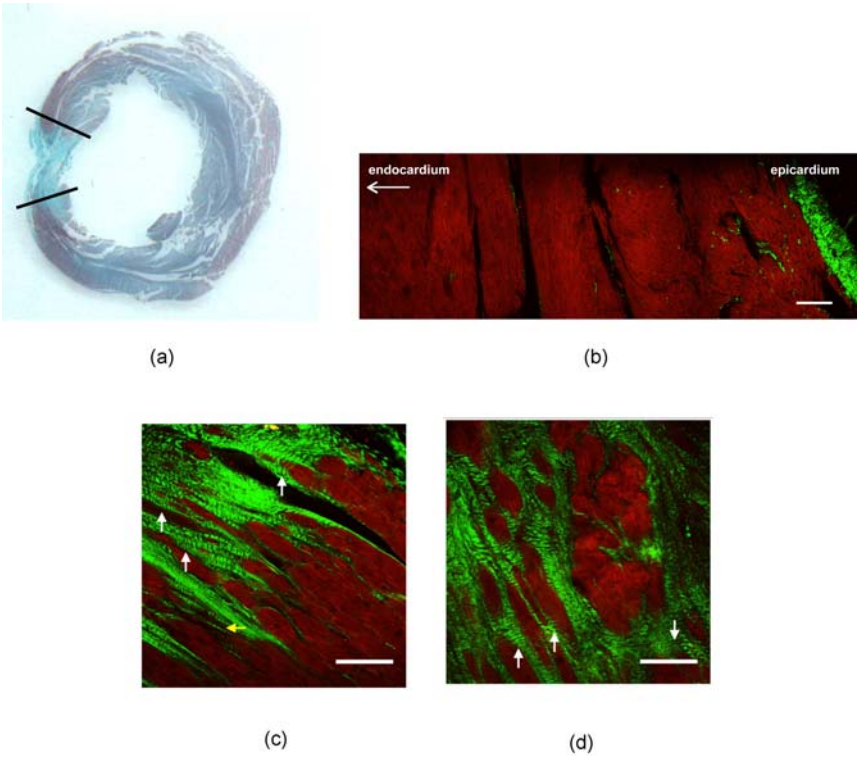

Figure 5 (online color at: www.biophotonics-journal.org) Stem-cell treated sample. (**a**) Histology (Masson's trichrome stain). The infarct is located between the bars. (**b**) Representative region away from site of infarct. (**c**) Site of infarct in a stem-cell treated heart. White arrows = sarcomeres; yellow arrows = striated collagen features. (**d**) Another representative image of the site of infarct after stem-cell treatment. Scale bars = 100 μm.

contrast to untreated hearts, we found a less sharp boundary between scar and healthy tissue, as well as many fewer regions entirely devoid of myocytes. Quantification of these regeneration changes (in terms of collagen and myocyte content and organization) would require imaging the entire scar, and will be reported in future studies.

4. Discussion

4.1 Characterization of the SHG signal

A few comments on the characterics of the SHG signal are warranted. SHG is known to preferentially emit in the foward direction. The magnitude of the foward/backward anisotropy is dependent on the size of the fibrils, with the largerst fibrils emitting considerably more SHG signal in the forward direction and smaller fibrils (≈ 40 nm diameter) showing an approximately equal forward/backward distribution [4]. As our setup collects SHG signal in backscatter geometry only, we may be somewhat more sensitive to contributions from immature collagen fibrils (which are smaller) than from larger fibrils.

SHG intensity is dependent on the angle between the collagen (or myosin) fibrils and the polarization plane of incident light [4]. The SHG signal is maximized when the incident light polarization and fibrils are parallel, and then gradually decreases and becomes quite small when they are perpendicular. For instance, studies in rat tail tendon [19] have found the intensity of SHG when the incident polarization and fibrils are parallel to be roughly four times larger than the intensity of SHG when they are perpendicular. Because the Chameleon laser used for this study is linearly polarized, we also observed a dependence of the intensity on the orientation of SHG-producing features. (No polarizers were used on the emission end, so that our collected signal is independent of the polarization of the emitted SHG signal.) Consistent with Freund et al. [19], we find that in highly aligned fibers such as those in Figure 4c, SHG signal undergoes a roughly four-fold change in intensity with sample rotation (data not shown). Because the SHG intensity of these fibers is quite high, however, we find that fibers remain visible in all orientations (i.e. visibility is maintained even at the orientation that yields lowest SHG signal). Furthermore, regions of disorganized collagen show lower dependence on sample orientation, with increases ranging from 50% to 150% between the sample positions producing minimum and maximum SHG intensities. This is due to the non-uniform orientation of individual fibrils in these regions. Note that while visualization of features was not impeded by the linear polarization of incident light, quantification of the SHG signal would be better performed with circularly-polarized light.

4.2 Injury and regeneration mechanisms

The results presented here are consistent with the known mechanisms of injury in infarcted myocardium, namely, the accumulation of scar tissue (collagen), tissue necrosis (decrease in viable myocytes), and adverse remodeling of tissue (thinning of the ventricular wall and disruption in the alignment and organization/orientation of remaining myocytes). Further, injection of mesenchymal stem cells has been shown to improve cardiac function in rats by preserving remote matrix architecture and preventing ventricular dilation [20]. These two-photon results support the hypothesis that both limitation of collagen accumulation in the scar and prevention of necrosis of myocytes in the infarct region may be potential mechanisms of functional improvement by stem-cell regeneration. Quantitative comparison of volumetric, wide field-of-view two-photon data could yield more information than histology while avoiding the potential distortion of samples associated with the very thin cuts necessary for histology.

4.3 Insights for tissue polarimetry

This study yields new insights into our ongoing polarimetric investigation of cardiac tissue. We have previously reported changes in the linear retardance of myocardial tissue in normal and infracted states using polarized light methods: infarcted hearts showed significantly decreased values of linear retardance in the infarct versus remote regions, with stem-cell treated hearts displaying a less severe reduction in linear retardance values [21, 22]. Figure 6 shows examples of linear retardance images for infarcted and stem-cell treated samples. As retardance reflects anisotropic tissue properties, these variations suggest underlying changes in the tissue structure. However, the underlying source of the retardance (and therefore, the exact cause of the retardance changes) was unclear.

Comparison of polarimetric and two-photon images reveals that tissue composition and organization (i.e. myocytes versus linear collagen versus wavy collagen) are reflected by linear retardance values. Specifically, myocytes are an important contributor to linear retardance, resulting in the high linear retardance exhibited in remote regions. Linear collagen regions such as the one seen in Figure 4c also exhibit high retardance, but wavy collagen regions such as the one seen in Figure 4d show low retardance, pre-

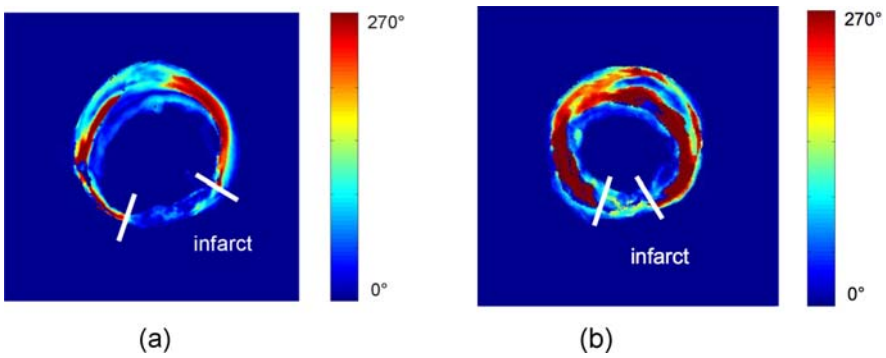

Figure 6 (online color at: www.biophotonics-journal.org) Polarimetry imaging (linear retardance) of infarcted (**a**) and stem-cell treated (**b**) rat myocardium. Color scale: linear retardance values (°) (measured in transmission through a 500 μm thick slice).

sumably because of the disarray of the fibers which results in a lower anisotropy. The infarct region in the sample shown in Figure 6a displayed mostly wavy collagen, hence the low retardance. The infarct region of the sample shown in Figure 6b displayed areas of high linear collagen content, resulting in patches of higher retardance in the scar region.

Furthermore, we find that in regions of high anisotropy (e.g., in regions containing either dense myocytes or linear collagen), measured linear retardance values also reflect the orientation of the anisotropy axis (the alignment of myocytes or collagen strands) with respect to the probing beam. For instance, the pattern visible on Figures 3b and 4b results in a low-high-low pattern of linear retardance from the inside to the outside of the ventricular wall (visible in the non-infarct regions of Figure 6a and b). This is consistent with expectations that the measured linear retardance should be maximal when the anisotropy axis is perpendicular to the probing beam (i.e., in the plane of imaging) and significantly lower as the two become more aligned [23].

This comparison suggests that the observed linear retardance decrease after infarct and increase after stem-cell treatment could be due to changes in tissue composition/organization (e.g., replacement of aligned myocytes with wavy collagen), due to changes in tissue orientation (e.g., from mostly perpendicular to mostly parallel with the probing beam), or due to a combination of these two effects. We have recently developed a method to remove this ambiguity and distinguish between the two effects by deriving both the magnitude *and* the orientation of tissue anisotropy [24, 25].

5. Conclusion

This work shows the first use of simultaneous two-photon autofluorescence and second-harmonic generation microscopy to image both the myocytes and the collagen components of healthy, infarcted and stem-cell regenerated heart, and provides further demonstration of the potential of simultaneous TPEF and SHG for endogenous cardiovascular imaging. Further, this study provides insight into our ongoing polarized-light work by shedding light on the underlying causes of the observed changes in quantified tissue anisotropy. Quantification of changes in composition and structure (collagen area/volume, myocyte transmural orientation, collagen organization/disarray) will require a larger field of view (ideally, whole-slide imaging) and volumetric data acquisition from thick tissue sections, and could provide additional information on the mechanisms of stem-cell cardiac regeneration.

Acknowledgements Support from the Natural Sciences and Engineering Research Council of Canada, the Canadian Institutes of Health Research (RMF 82498 to Drs Vitkin and Li, and MOP 102535 to Dr. Li) and the Canada Foundation for Innovation is gratefully acknowledged.

Marika A. Wallenburg obtained her B.Sc. from McGill University in Physics in 2008 and has just completed an M.Sc. in Medical Biophysics at the University of Toronto. She ist the recipient of an NSERC Postgraduate Scholarship. Her work focusses on the use of two-photon microscopy and polarimetry for cardiac tissue imaging. This is her third first-author publication.

Jun Wu, M.D., M.Sc., is a research technician and animal research manager in the Department of Cardiovascular Research at the Toronto General Hospital. He received his Masters and M.D. degree from China. As part of Dr. Li's laboratory, his

work is focused on finding optimal cell types and times for transplantation into the heart after myocardiol infarction, and describing the optimal conditions under which the transplanted cells can achieve the most efficient repair.

Dr. Ren-Ke Li, M.D., Ph.D., is a Professor of Medicine in the Department of Surgery, Division of Cardiovascular Surgery and Department of Laboratory Medicine and Pathobiology at the University of Toronto and a Senior Scientist at the Toronto General Research Institute, University Health Network. He is the recipient of the Canada Research Chair in Cardiac Regeneration and a Career Investigator of the Heart and Stroke Foundation of Canada. Dr. Li has published 145 peer-reviewed papers.

Alex Vitkin, Ph.D. is an engineering physicist/biomedical engineer. He is currently Professor of Medical Biophysics and Radiation Oncology at University of Toronto, a Senior Scientist at the Ontario Cancer Institute, and a Medical Physicist at Princess Margaret Hospital, Toronto, Canada. His research is in the field of biophotonics, with particular emphasis on Doppler optical coherence tomography, tissue polarimetry, and optical fiber sensors. Dr. Vitkin has published ~100 peer-reviewed scientific papers.

References

[1] K. Schenke-Layland, I. Riemann, U. Stock, and K. Konig, J. Biomed. Opt. **10**, 024017 (2005).
[2] A. Zoumi, X. Lu, G. Kassab, and B. Tromberg, Biophys. J. **87**(4), 2778–2786 (2004).
[3] S. Wallace, J. Morrison, K. Botting, and T. Kee, J. Biomed. Opt. **13**, 064018 (2008).
[4] R. Williams, W. Zipfel, and W. Webb, Biophys. J. **88**(2), 1377–1386 (2005).
[5] S. Plotnikov, A. Millard, P. Campagnola, and W. Mohler, Biophys. J. **90**(2), 693–703 (2006).
[6] S. Plotnikov, A. Kenny, S. Walsh, B. Zubrowski, C. Joseph, V. Scranton, G. Kuchel, D. Dauser, M. Xu, C. Pilbeam, D. Adams, R. Dougherty, P. J. Campagnola, and W. A. Mohler, J. Biomed. Opt. **13**, 044018 (2008).
[7] T. Ragan, J. Sylvan, K. Kim, H. Huang, K. Bahlmann, R. Lee, and P. So, J. Biomed. Opt. **12**, 014015 (2007).
[8] H. Huang, C. MacGillivray, H. Kwon, J. Lammerding, J. Robbins, R. Lee, and P. So, J. Biomed. Opt. **14**, 044029 (2009).
[9] K. Schenke-Layland, U. Stock, A. Nsair, J. Xie, E. Angelis, C. Fonseca, R. Larbig, A. Mahajan, K. Shivkumar, M. Fishbein, and W. R. MacLellan, Eur. Heart J. **30**(18), 2254 (2009).
[10] M. Tsai, Y. Chiou, and C. Sun, Proc. SPIE **7161**, 71612O (2009).
[11] M. Matsumoto-Ida, M. Akao, T. Takeda, M. Kato, and T. Kita, Circulation **114**(14), 1497 (2006).
[12] J. Sun, S. Li, S. Liu, J. Wu, R. Weisel, Y. Zhuo, T. Yau, R. Li, and S. Fazel, Am. J. Physiol-Heart C **296**(1), H43 (2009).
[13] W. Zipfel, R. Williams, R. Christie, A. Nikitin, B. Hyman, and W. Webb, Proc. Natl. Acad. Sci. USA **100**(12), 7075 (2003).
[14] G. Cox, E. Kable, A. Jones, I. Fraser, F. Manconi, and M. Gorrell, J. Struct. Biol. **141**(1), 53–62 (2003).
[15] E. Brown, T. McKee, E. diTomaso, A. Pluen, B. Seed, Y. Boucher, and R. K. Jain, Nat. Med. **9**(6), 796–800 (2003).
[16] A. Pope, G. Sands, B. Smaill, and I. LeGrice, Am. J. Physiol. Heart Circ. Physiol. **295**(3), H1243 (2008).
[17] G. Bub, P. Camelliti, C. Bollensdorff, D. Stuckey, G. Picton, R. Burton, K. Clarke, and P. Kohl, Am. J. Physiol. Heart Circ. Physiol. **298**(5), H1616 (2010).
[18] M. Both, M. Vogel, O. Friedrich, F. von Wegner, T. Kunsting, R. Fink, and D. Uttenweiler, J. Biomed. Opt. **9**, 882 (2004).
[19] I. Freund, M. Deutsch, and A. Sprecher, Biophys. J. **50**(4), 693–712 (1986).
[20] P. Farahmand, T. Lai, R. Weisel, S. Fazel, T. Yau, P. Menasche, and R. Li, Circulation **118**(suppl 1), S130 (2008).
[21] N. Ghosh, M. F. G. Wood, S. Li, R. D. Weisel, B. C. Wilson, R. K. Li, and I. A. Vitkin, J. Biophotonics **2**(3), 145–156 (2009).
[22] M. F. G. Wood, N. Ghosh, M. A. Wallenburg, S. Li, R. D. Weisel, B. C. Wilson, R. K. Li, and I. A.Vitkin, J. Biomed. Opt. **15**, 047009 (2010).
[23] B. E. A. Saleh and M. C. Teich, Fundamentals of Photonics (John Wiley & Sons, New York, 1991).
[24] M. A. Wallenburg, M. Pop, M. F. G. Wood, N. Ghosh, G. A. Wright, and I. A. Vitkin, J. Innov. Opt. Health Sci. **3**(2), 109–121 (2010).
[25] M. A. Wallenburg, M. Wood, N. Ghosh, and I. A. Vitkin, Opt. Lett. **35**, 2570–2572 (2010).

